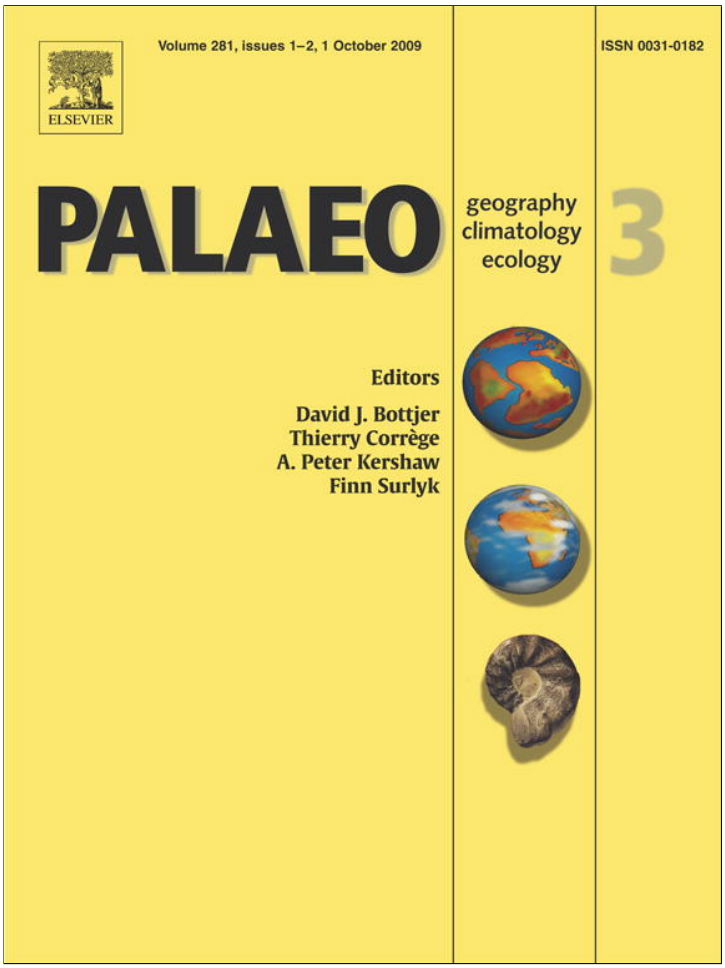

Palaeogeography, Palaeoclimatology, Palaeoecology 281 (2009) 57–65

Contents lists available at ScienceDirect

Palaeogeography, Palaeoclimatology, Palaeoecology

journal homepage: www.elsevier.com/locate/palaeo

Refining a pedogenic-carbonate CO_2 paleobarometer to quantify a middle Miocene greenhouse spike

Gregory J. Retallack

Department of Geological Sciences, University of Oregon, Eugene OR U.S.A. 97403, United States

ARTICLE INFO

Article history:
Received 17 April 2009
Received in revised form 7 July 2009
Accepted 18 July 2009
Available online 28 July 2009

Keywords:
Paleosol
Carbon dioxide
Greenhouse
Miocene
Idaho
Montana

ABSTRACT

Estimates of respired soil CO_2 concentration in paleosols are needed to calculate past atmospheric CO_2 levels from the difference between organic and carbonate carbon isotopic values in paleosols. A new compilation of CO_2 concentrations late in the growing season in modern calcareous soils can be used to estimate respired soil CO_2 by subtracting atmospheric CO_2 concentrations. Furthermore, respired CO_2 shows a significant relationship with depth to calcic horizon, and this relationship can be used to estimate respired CO_2 concentrations in paleosols. These values, as well as estimates of $\delta^{13}C$ of atmospheric CO_2 from $\delta^{13}C$ of soil organic matter, and of paleotemperature from Bw horizon chemical composition, refine the Cerling CO_2 paleobarometer. These refinements are applied to quantify the middle Miocene greenhouse, which has been controversial because it was not detected by marine alkenone and boron paleobarometers. New estimates of middle Miocene atmospheric CO_2 from paleosols in Railroad Canyon, Idaho, reveal levels at 16 Ma of 852 ± 86 ppmv. This is similar to predicted values by 2100, and 3 times pre-industrial values (PIL = 280 ppmv).

1. Introduction

By the year 2100, atmospheric CO_2 concentrations are predicted to triple, from pre-industrial levels of 280 ppmv to some 856 ppmv (+70/−101 ppmv) based on scenario A2 of a very heterogeneous world with continued population growth (Alley et al., 2007). Such changes are unprecedented in Quaternary records, but their effects can be assessed by proxies for atmospheric CO_2 deeper in geological time (Royer et al., 2001) using mass balance models of sedimentary carbon and sulfur (Berner, 1997, 2006), algal carbon isotope composition (Pagani et al., 1999; Kaufman and Xiao, 2003; Pagani, 2002), foraminiferal boron isotope composition (Pearson and Palmer, 1999, 2000), stomatal index of fossil plants (McElwain et al., 1999; Retallack, 2002), goethite-occluded carbonate in paleosols (Yapp and Poths, 1992; Tabor and Yapp, 2005), base depletion of paleosols (Sheldon, 2006a, 2006c), strontium isotopic values of marine carbonates (Rothman, 2002), and carbon isotopic values of pedogenic carbonate (Cerling, 1991; Sheldon and Tabor, 2009). This paper refines this last technique, which has been widely applied to paleosols (Ekart et al., 1999; Nordt et al., 2003, Montañez et al., 2007), and which can potentially be employed back at least to 2.6 Ga (Watanabe et al., 2000).

Cerling's (1991) model for paleosols exploits the marked difference in isotopic compositions of carbon in CO_2 of the atmosphere (about −6.5‰ $\delta^{13}C$), and CO_2 produced by soil respiration and oxidation of C3 plants (about −26‰ $\delta^{13}C$). As levels of atmospheric CO_2 rise, higher partial pressure of isotopically heavy atmospheric CO_2 offsets isotopically light respired CO_2, and the carbon isotopic value fixed within low magnesium calcite of soil carbonate also rises. Until now only plausible ranges of respired CO_2 and sensitivity analysis could be applied (Mora et al., 1991; Montañez et al., 2007; Breecker et al., 2009). Compilations of global soil data (Brook et al., 1983) reveal that soil CO_2 is strongly related to mean annual precipitation (MAP) and mean annual temperature (MAT). Soil data presented here, now provide transfer functions for estimating respired CO_2 levels from depth to calcareous nodules (Bk horizon of Soil Survey Staff 2000). Two additional refinements are (1) calculating atmospheric CO_2 isotopic composition from paleosol organic matter (Arens et al. 2000), as done by Nordt et al. (2003), and (2) calculating paleotemperature from paleosol chemical composition, as done by Sheldon et al. (2002).

These refinements are applied to an example calculation of the middle Miocene global greenhouse, which has proven controversial, because stomatal-index data suggest a significantly higher than modern level of middle Miocene CO_2 (Retallack, 2002; Kürschner et al., 2008), whereas algal alkenone (Pagani, 2002) and foraminiferal boron (Pearson and Palmer, 1999) paleobarometers suggest lower than modern middle Miocene CO_2. Because there is widespread independent evidence of higher than modern middle Miocene temperature and precipitation (Zachos et al., 2001; Bruch et al., 2007; Retallack, 2007), the low alkenone and boron estimates have been taken as evidence of CO_2–climate uncoupling (Cowling, 1999). These discrepancies are thus a challenge to CO_2-greenhouse theory, which guides prediction of future global warming (Alley et al., 2007).

E-mail address: gregr@darkwing.uoregon.edu.

0031-0182/$ – see front matter © 2009 Elsevier B.V. All rights reserved.
doi:10.1016/j.palaeo.2009.07.011

2. Materials and methods

Refinement of the pedogenic CO_2 paleobarometer of Cerling (1991) proposed here comes from a literature compilation of growing-season CO_2 levels measured within soils. These data are now much more copious than for the earlier compilation of Brook et al. (1983: see also Supplementary data). This study focuses on a subset of these data consisting of all published CO_2 measurements from calcic and gypsic soils distributed around the world (Fig. 1). Many of these observations of soil CO_2 come from continuously monitored sites revealing seasonal variations (Fig. 2). These data are here used as the basis of transfer functions (Fig. 3) useful for interpreting paleosols.

As a worked example, the refined Cerling (1991) model is applied to middle Miocene paleosols in Railroad Canyon, Idaho. Fieldwork there consisted of measuring the depth to Bk as a proxy for paleoprecipitation, Munsell color, and also thickness of paleosol with calcareous nodules as a proxy for paleoseasonality (Retallack, 2005) within stratigraphic sections measured by the method of eyeheights (Retallack, 2007). These data have been conformed to the same datum as a recent composite section and magnetostratigraphy (modified from Barnosky et al. 2007), and stratigraphic levels of pedogenic carbonate stable isotopic analyses (Kent-Corson et al. 2006).

3. Refining a pedogenic CO_2 paleobarometer

3.1. Introduction

The Cerling (1991) pedogenic carbonate CO_2 paleobarometer is based on the very different carbon isotopic composition of CO_2 in the atmosphere and respired within soils, which can be mixed in various proportions at different times of year and depth within soils. The fundamental equation of the paleobarometer is as follows (Ekart et al., 1999).

$$P_a = P_r \cdot \frac{(\delta^{13}C_s - 1.0044\delta^{13}C_r - 4.4)}{(\delta^{13}C_a - \delta^{13}C_s)} \quad (1)$$

Variables in this equation are partial pressures of CO_2 (P in ppmv), and carbon isotopic values of carbon in CO_2 ($\delta^{13}C$ in ‰). Subscripts are in atmosphere (a), in soil (s), and respired in soil (r). These values in turn are derived from measured carbon isotopic compositions of pedogenic carbonate ($\delta^{13}C_c$) and organic matter ($\delta^{13}C_o$) in paleosols. For example, $\delta^{13}C_r$ is approximated by $\delta^{13}C_o$ (Cerling 1991). The concentration of respired soil CO_2 (P_r in Eq. (1)) is a controlling variable, and until now its value could only be guessed for paleosols based on estimates from comparable modern soils (Montañez et al., 2007; Sheldon and Tabor 2009). A proxy for paleosol respired CO_2 is needed.

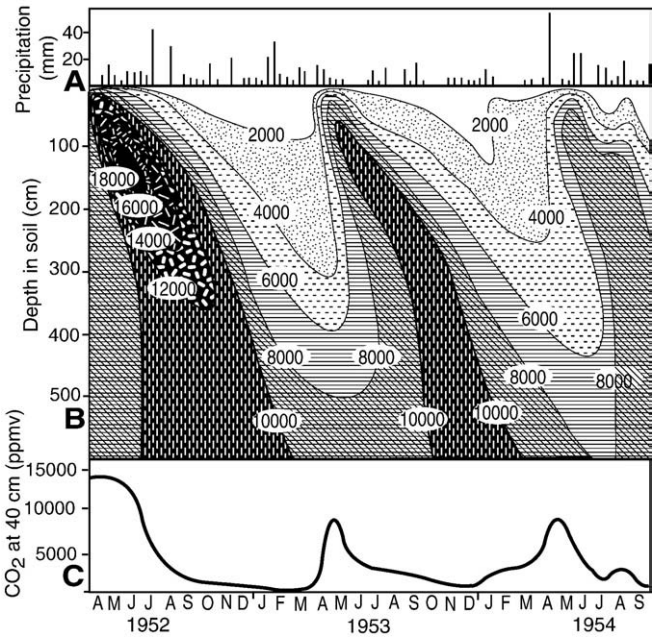

Fig. 2. Precipitation events in mm (A), contoured soil CO_2 concentrations in ppmv for various times or year and depth within soil (B), and concentrations of CO_2 in ppmv at 40 cm depth of Bk (C) over three successive years in a soil near El'ton, Kazakhstan (redrafted from Matsevich, 1957).

3.2. A new proxy for CO_2 respired by paleosols

Soil CO_2 is derived in part from the atmosphere and in part from respiration of roots, animals and microbes, and can reach levels up to 104,000 ppmv in tropical rain forest soils (371 times CO_2 concentrations in the pre-industrial atmosphere: Matsumoto et al., 1997). The lowest CO_2 concentrations in soils are nearest to the surface, where atmospheric CO_2 sets a minimum level (Cerling, 1991). The highest CO_2 concentrations are deep within soils, where microbes and roots respire within small pores with tortuous diffusion paths to the atmosphere. The zone of maximal CO_2 is within 1–2 m of the surface after growing-season rains, but migrates deeper within the soil in snowy or dry seasons (Fig. 2A: Matsevich, 1957; Buyanovsky, 1972; Buyanovsky et al., 1982). Soil CO_2 dissolves in soil water to form

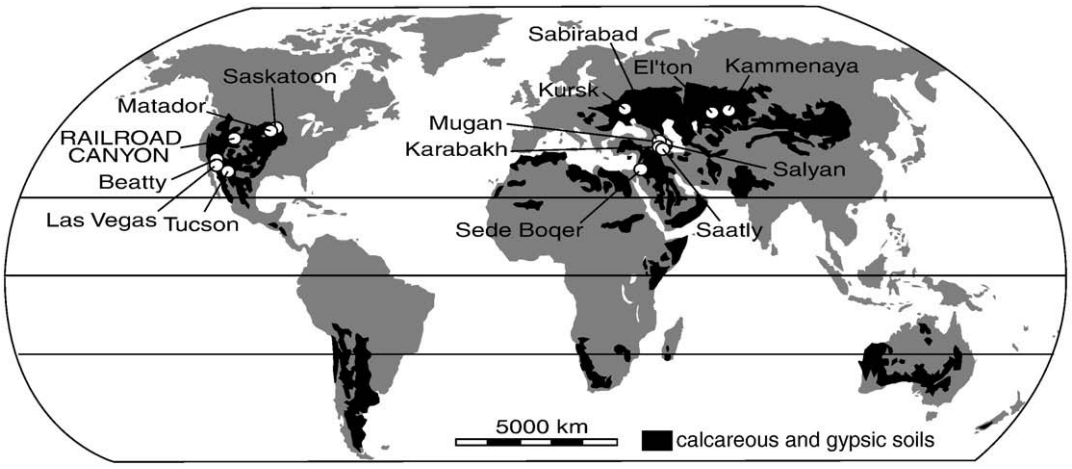

Fig. 1. Location of Railroad Canyon, Idaho, and of experiment stations for calcareous soil CO_2, on a global map of calcareous soils.

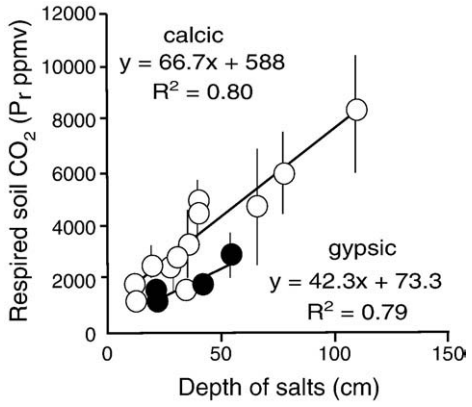

Fig. 3. Relationships between late growing season respired soil CO_2 and depth to calcic (open circles) and gypsic (closed circles) horizons in soils. Standard error for the calcic relationship is = ±893 ppmv, and for the gypsic relationship is ±431 ppmv.

carbonic acid responsible for hydrolytic weathering and carbonate dissolution (Brook et al., 1983), but alkaline earth cations mobilized early in the growing season are precipitated as dolomite or low-magnesian calcite nodules later in the growing season in arid to subhumid soils (McFadden and Tinsley, 1985). At the level of caliche nodules (0.4 m in Fig. 2B) soil CO_2 rises following a flush of productivity following growing-season rains, then falls after the growing season (Fig. 2C).

Among the various levels of soil respiration observed during a year, late growing-season values match best model assumptions of the pedogenic carbonate CO_2 paleobarometer (Cerling, 1991). In temperate aridland soils, the first flush of early growing-season soil respiration and rain promotes dissolution over precipitation of carbonate and little or no intrusion of atmospheric CO_2, but during the dry–cold season there is little dissolution or precipitation and atmospheric CO_2 penetrates more deeply into hibernating soil (Quade et al., 1989). During the late growing season in contrast, there is a shoulder of soil respiration when soils show modest atmospheric intrusion, and this is the time when Ca^{2+} ions in soil solution show the most rapid decline, indicating carbonate precipitation (Breecker et al., 2009). There also is a marked decline in Ca^{2+} ions after the first spring rains, but that carbonate is prone to dissolution during the main growing-season peak of soil CO_2. Thus the late growing-season shoulder in soil CO_2 concentration (Fig. 2C) is the best approximation to concentration during long-term carbonate nodule precipitation.

Controls on seasonal and regional variation in soil CO_2 levels and carbonate precipitation are comparable with controls in soil productivity, such as temperature and precipitation (Lieth and Whitakker, 1975). Significant relationships between mean growing-season soil CO_2 and mean annual temperature, precipitation, and evapotranspiration have been demonstrated by Brook et al. (1983), but were not improved by my compilation of much additional soil CO_2 data (see Supplementary data). Nor were these relationships improved by calculating the respired component of soil CO_2 by subtracting the measured atmospheric CO_2 for the month and year of observation (data from website ftp://ftp.cmdl.noaa.gov/ccg/co2/trends/co2_annmean_mlo.txt: accessed Jan 14, 2009). These website data document anthropogenic rise of atmospheric CO_2 levels since 1958, and monthly levels for that year were used to calculate respired CO_2 for prior experimental observations (Fig. 2).

My data compilation did yield a novel and highly significant relationship between (1) late growing season (late July–early September) respired CO_2 at moderate depths (30–60 cm) and (2) depth to Bk horizon (Fig. 3). This latter is the depth, not to the highest nodule, but to the level where nodules mark a distinct change in horizon character (Retallack, 2005). Although soils can have shallower and deeper Bk horizons, they were not found in the literature compilation used here of soil CO_2 measurements from 15 modern calcareous soils (Matsevich, 1957; Buyanovsky, 1972; de Jong and Schappert, 1972; de Jong, 1981; Buyanovsky et al., 1982; Parada et al., 1983; Quade et al., 1989; Breecker et al., 2009). Not all these studies documented depth to calcic horizon, but that information is available elsewhere (Dan et al., 1973; Clayton et al., 1977; Salayev, 1985; Mikhailova et al., 2000; Torn et al., 2002; Cochran and Richardson, 2003; Borup, 2004; Demkin et al., 2006). Most of these soils furnished several measurements from continuous monitoring over several seasons, and the total number of late growing-season CO_2 measurements in the database is 162. A similar relationship was also found between soil CO_2 and depth to gypsum in 8 measurements from 4 gypsic soils (Fig. 3), whose By horizons were documented (Dan et al., 1973; Quade et al., 1989; Borup, 2004). Some of these soils have both a Bk horizon, and a deeper By horizon, so that the P_r–By relationship may provide a useful check on respired CO_2 levels of comparable paleosols. Soil respiration levels of gypsic soils are also of interest for reconstructing productivity of Cambrian and Precambrian paleosols (Retallack, 2008).

The two new transfer functions between respired soil CO_2 (P_r in ppmv) and depth to carbonate (D_s in cm) and to gypsum (G_s in cm) are significant ($R^2 = 0.80$, S.E. ± 893 ppmv for Eq. (2), and $R^2 = 0.79$, S.E. ± 431 ppmv for Eq. (3)), and given below.

$$P_r = 66.7D_s + 588 \quad (2)$$

$$P_r = 42.3G_s + 73.3 \quad (3)$$

Scatter in these relationships may be due to local variation in Bk depth, which reflects long-term (10^3–10^5 years) soil formation, rather than rainfall and respiration pulses over weeks and years of monitored observations (Fig. 2). Similar temporal scaling problems limit significance of larger databases for the relationship between depth to Bk and mean annual precipitation in soils (Retallack, 2005).

These calcic and gypsic proxies for paleosol CO_2 are of broad application to paleosols, because the database is global and includes both moderate and low latitudes, as well as ustic (winter dry) and xeric (summer dry) moisture regimes (Fig. 1). The database includes sandy and gravelly soils from Arizona, New Mexico and Nevada, and loess soils from Canada, Israel and central Asia. All the soils in the calibrating climosequence had carbonate in powdery, clast-pendant or nodular form and represent geomorphic surfaces no older than late Pleistocene (see Supplementary data).

The greatest limitation for application of these proxies to paleosols is compaction of soils during burial, so that depth to Bk in paleosols (D_p in cm) is less than depth in the original soil (D_s in cm). Original depth can be calculated directly by ptygmatic folding of formerly planar features in paleosols, but also can be calculated from estimated thickness of overburden (K in km) using a standard compaction formula for Aridisols (Sheldon and Retallack 2001), as follows.

$$D_s = D_p / \left[-0.62 / \left(\frac{0.38}{e^{0.17K}} - 1 \right) \right] \quad (4)$$

Another limitation for application of these proxies to paleosols is erosion before burial, which can be assessed in several ways. Fossil roots converging to trunks in the surface of a paleosol are especially convincing evidence against erosion, and paleosols with near-planar tops in aggrading loess sequences also are unlikely to be eroded (Retallack 1997). Silty paleosols truncated by sandstone paleochannels are suspect (Retallack 1997), as are paleosols with tabular Bk horizons formed over soil durations of more than 10,000 years (Retallack 2005). Soils and paleosols with carbonate deeper than 110 cm and gypsic horizons deeper than 60 cm exceed limits of the climosequence. Use of this proxy for soil CO_2 in frigid, tropical and monsoonal climates is also an extrapolation from available data (Fig. 1), but calcic–gypsic soil-CO_2 is well within the array of CO_2

concentrations in non-calcic and non-gypsic soils from these climatic extremes (Brook et al., 1983; see Supplementary data). Paleosols developed on bedrock or very clayey substrates should be excluded because unrepresented in the climosequence.

3.3. Published proxies for atmospheric $\delta^{13}C$

Another complication for the Cerling (1991) paleobarometer is temporal variation in carbon isotopic values of atmospheric CO_2. A useful proxy for atmospheric $\delta^{13}C$ ($\delta^{13}C_a$ in ‰) is isotopic composition of organic matter ($\delta^{13}C_o$ in ‰), according to the following equation ($R^2 = 0.34$, S.E. = ± 0.4‰: from Arens et al., 2000).

$$\delta^{13}C_a = \frac{\delta^{13}C_o + 18.67}{1.1} \quad (5)$$

Fossil plants from coal or leaf beds interbedded with paleosols have been used for this purpose (Montañez et al., 2007), but can be misleading because coal and plant preservation is favored by wet, warm, and high-CO_2 times of climatic cycles (Retallack, 2007). Fossil humus in well drained calcareous paleosols may be strongly fractionated by aerobic decay, so that analysis of depth functions of isotopic composition may be needed to extrapolate original organic carbon isotopic values (Wynn, 2007). Alternatively, organic carbon occluded in biomineralized woody seeds from paleosols may be used (Backlund et al., 1991), but this is seldom sufficiently abundant in every paleosol to construct geological time series. An alternative approach is to model variation in $\delta^{13}C$ of atmospheric CO_2 through geological time from high resolution marine isotopic records, adjusted to local circumstances by empirical fractional factors (Passey et al., 2002; Nordt et al., 2003).

3.4. Published proxies for soil paleotemperature

Carbon isotopic composition of soil CO_2 ($\delta^{13}C_s$ in ‰) and soil carbonate ($\delta^{13}C_c$ in ‰) is also dependent on temperature (T in °C) of crystallization (Romanek et al., 1992), according to the following relationship ($R^2 = 0.93$, S.E. = 0.28‰).

$$\delta^{13}C_s = \frac{\delta^{13}C_c + 1000}{\frac{11.98 - 0.12 \cdot T}{1000} + 1} - 1000 \quad (6)$$

Deriving paleotemperature from isotopic composition of oxygen ($\delta^{18}O$) in soil carbonate (Dworkin et al., 2005) or clays (Tabor, 2007) may be difficult because of metamorphic alteration of paleosols (Mora et al., 1998), or because of orographic rain-shadow effects (Kent-Corson et al., 2006). Modern surface domains of $\delta^{18}O$ and δD in clays can be used to constrain rain-shadow effects in intermontane paleosols (Tabor and Montañez, 2005). The clumped-isotope carbonate paleothermometer (Ghosh et al., 2007) is very promising, but requires calibration for paleosols. Paleosol mean annual paleotemperature can be derived from a clayeyeness chemical ratio for Inceptisols (Sheldon, 2006b). The most suitable paleotemperature proxy for Aridisols is an alkali ratio ($A = (Na_2O + K_2O)/Al_2O_3$, as a molar ratio), which is related to mean annual temperature (T in °C), by the following equation ($R^2 = 0.37$; S.E. = ± 4.4 °C; Sheldon et al., 2002).

$$T = -18.5A + 17.3 \quad (7)$$

4. Middle Miocene CO_2 example

4.1. Calcareous paleosols in Railroad Canyon, Idaho

Calcareous paleosols of the kind needed for application of the Cerling (1991) CO_2 paleobarometer are widespread in Railroad Canyon, Idaho (Figs. 4–5), an area of Barstovian fossil mammal localities (Barnosky et al., 2007). These paleosols have been the focus of stable isotopic (Kent-Corson et al., 2006), paleopedological, and major element geochemical studies (Retallack, 2007).

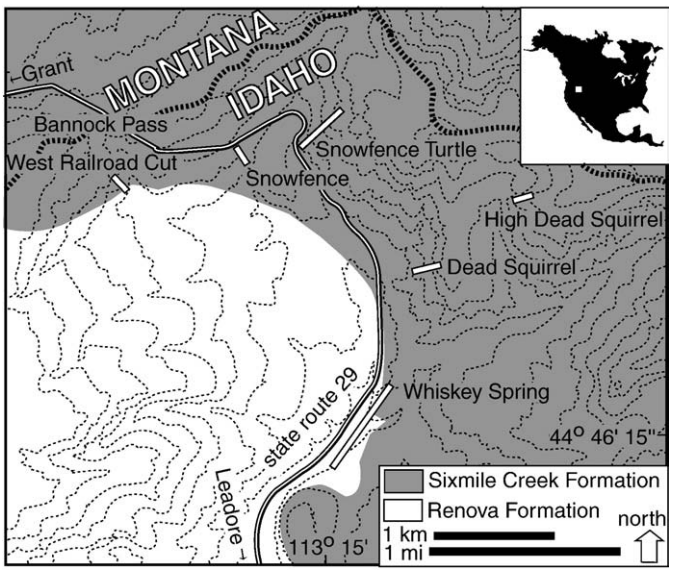

Fig. 4. Geological map and localities for paleosols examined in Railroad Canyon, Idaho (after Barnosky et al., 2007).

The most prominent lithological change in the section is from pale olive-gray Renova Formation below to brown Sixmile Creek Formation above (Figs. 4–5). This contact has been regarded as a regional "unconformity" (Barnosky et al., 2007), and is certainly a shift in paleoclimatically sensitive features of paleosols such as depth to Bk (Fig. 6). However, the age of the regional unconformity has been revised from 16 Ma (early Barstovian) to 20 Ma (early Hemingfordian: Hanneman and Wideman, 2006). There is no detectable angular discordance or paleovalley development at this stratigraphic level in Railroad Canyon, which was presumably a local depocenter little affected by basin margin discordance. Late Hemingfordian fossil mammals, not much older than Barstovian, were not found in Railroad Canyon, but are known from the Renova Formation in Maiden Creek, 11 km to the north (Retallack, 2007), and Mollie Gulch 12 km to the southwest (Barnosky et al., 2007). The Renova–Sixmile contact is thus stratigraphically higher than the regional early Hemingfordian hiatus (Hanneman and Wideman, 2006), but was nevertheless avoided in the following reconsideration of local magnetostratigraphic dating.

4.2. New age model for Railroad Canyon magnetostratigraphy

The time scale of Cande and Kent (1995) used by Barnosky et al. (2007) for magnetostratigraphic dating of the Railroad Canyon section can now be updated using recent revisions by Ogg and Smith (2004). Levels from the "basic unrevised" magnetostratigraphy of Barnosky et al. (2007) are here plotted against 16 different sets of revised chron ages: in essence, sliding the standard time scale against the proportional thicknesses of magnetozones in Railroad Canyon to determine the best fit (Fig. 7). All but 3 of the 16 alternatives can be rejected using biostratigraphic data. Diverse and definitive Barstovian faunas between 140 and 230 m in the section are no older than 16 Ma and no younger than 12.5 Ma (Tedford et al., 2004). Fossils are sparse above and below that level, so biostratigraphically unconstrained (Barnosky et al. 2007). The three acceptable models date the base of the normal immediately above the base of the Sixmile Creek Formation at 16.721, 16.472 and 16.268 Ma respectively. Two of these age models (starting at 16.721 and 16.472 Ma) can be rejected because of tephrostratigraphic correlation of a peralkaline ash at 23 m in Railroad Canyon with a 16.6–15.8 Ma ash from McDermitt, Oregon

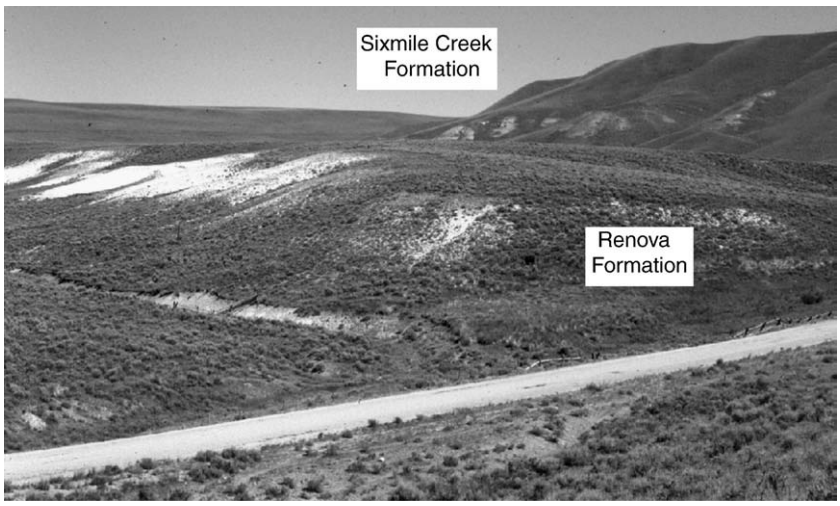

Fig. 5. View up Railroad Canyon from the eastern end of Whiskey Spring section (Fig. 4). Pale olive (5Y6/3) deep-calcic, clayey paleosols of the Renova Formation, contrast with light yellowish brown (2.5Y6/3), silty paleosols of the overlying Sixmile Creek Formation.

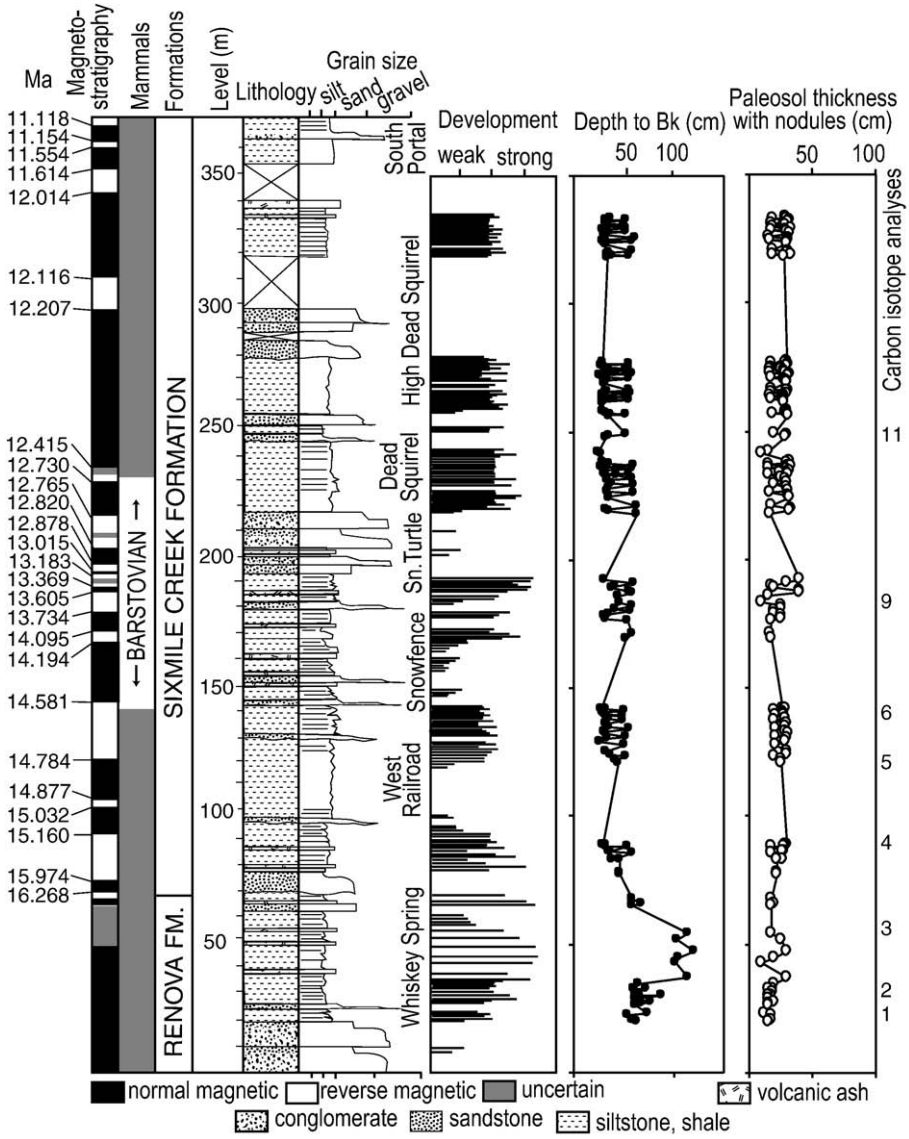

Fig. 6. Composite section and magnetostratigraphy of Railroad Canyon modified from Barnosky et al. (2007), with degree of paleosol development, depth to calcareous nodules and thickness of soil with calcareous nodules. Carbon isotope sample numbering follows Kent-Corson et al. (2006).

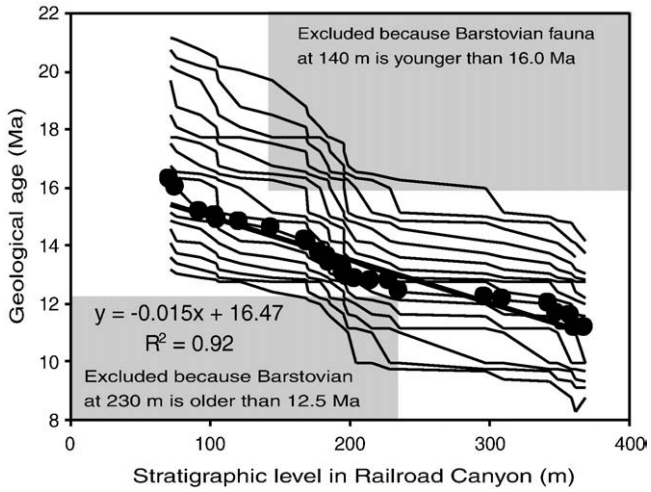

Fig. 7. Revised age model for Railroad Canyon magnetostratigraphy, using new chron dating (Ogg and Smith, 2004), and biostratigraphic constraints (Barnosky et al., 2007).

(Barnosky et al., 2007). These same two models can also be rejected for lower correlation than the age model chosen, which shows least variation in sedimentation rate. The 16.721 Ma option adopted by Barnosky et al. (2007) disregards 4 normals between 184 and 228 m, and casts doubt on the ash correlation. By the new age model (Fig. 7) the reversed interval from 76 to 93 m in Railroad Canyon (Fig. 6) correlates with interval R3 at Hepburns Mesa near Yellowstone National Park, Wyoming, which probably includes a 15.82 ± 0.21 Ma ash low in a section 6 km to the north east of the paleomagnetically-studied section (Barnosky and Labar, 1989). Also correlative further afield are a reversed interval with 16.2 ± 1.4 Ma and 15.8 ± 0.07 Ma ashes near Dayville, Oregon (Prothero et al., 2006), and interval R6 including the 15.88 ± 0.06 Ma Oreodont tuff near Barstow, California (Burbank and Barnosky, 1990).

4.3. Suitability of Railroad Canyon paleosols for CO_2 estimates

Middle Miocene paleosols of Railroad Canyon are mostly Aridisols with A-Bk profiles. They have silty, rhyodacitic tuffaceous parent materials from rapidly aggrading floodplains, and their nodules are mostly smaller than those in Holocene soils (Retallack, 2005). Some of the deep-Bk paleosols of the upper Renova Formation have large nodules, and may represent longer periods of soil formation, but as with the shallow-Bk paleosols, there is no evidence of pre-burial erosion that might affect use of Bk depth as a proxy for soil CO_2 (Retallack, 2007). This part of Idaho during the Miocene was mountainous and at its current latitude (Kent-Corson et al., 2006), appropriate to the distribution of modern soil data (Fig. 1). Overburden to this sequence was about 0.7 km (Hanneman and Wideman, 2006), so that the paleosols have been significantly compacted by overburden (Sheldon and Retallack, 2001), but remain friable and unmetamorphosed. Nevertheless, their oxygen isotopic values (Table 1) are significantly lower (by −7 to −10‰) than for Early Eocene paleosols of the same region. Kent-Corson et al. (2006) argue that this distinct isotopic shift marks onset of a pronounced orographic rain-shadow effect, which would compromise paleotemperature estimates from oxygen isotopic data. This leaves alkali index most appropriate for calculating paleotemperatures (Sheldon et al., 2002). Carbon isotopic values of Railroad Canyon pedogenic carbonate (Table 1) are all as expected for C_3 rather than C_4 parent vegetation (for comparator values from Miocene paleosols, see Behrensmeyer et al., 2007). Idaho is too far north and west for C_4 plants today (Sage et al., 1999), and Railroad Canyon paleosols predate by about 10 Ma the advent of C_4 vegetation in the Great Plains of North America (Passey et al., 2002). There is no evidence that C_4 vegetation was introduced into Idaho during the middle Miocene warm–wet spike.

4.4. New middle Miocene atmospheric CO_2 estimates

Of the various carbon isotopic compositions needed for the pedogenic carbonate CO_2 paleobarometer (Eq. (1)), isotopic composition of pedogenic carbonate (C_c) was measured from paleosols in Railroad Canyon by Kent-Corson et al. (2006). Two other quantities ($\delta^{13}C_a$ and $\delta^{13}C_r$) can be derived from carbon isotopic composition of organic matter ($\delta^{13}C_o$), which should be roughly −22‰ from geographic gradient analysis of middle Miocene hackberry seeds in paleosols of the northern Great Plains (Backlund et al., 1991). This is the same as values for water-stressed C3 vegetation calculated for 0.5 Ma intervals of the Miocene (Table 1) using known fractionations from marine isotopic data by Passey et al. (2002). Paleosol depth to Bk, burial depths, and alkali paleotemperature are as previously published (Retallack, 2007).

As an example calculation, consider the paleosol at the middle Miocene CO_2 maximum (Table 1). This paleosol is at 58 m in the section, and thus 15.61 Ma in the age model of Fig. 7. Its Bk horizon is below 115 cm of near-mollic, pale olive (5Y6/3) claystone, in turn overlain by laminated white (5Y8/1) volcanic ash (Retallack, 2007). The depth to Bk would have been 125 cm before burial compaction under 0.86 km of local overburden (Retallack, 2007), following Eq. (4) (from Sheldon and Retallack, 2001). The equation for Aridisols was used despite the depth to Bk greater than 1 m, because the profile has a Bk horizon more strongly developed than Inceptisols, and does not have the organic or structural character of a deep Mollisol (tall grass prairie soil), which evolved later in geological time (Retallack, 2007). This original depth is also an extrapolation from the training set for Eq. (2) (up to 110 cm only), but was used to calculate a late

Table 1
Data used to calculate middle Miocene atmospheric CO_2 (ppmv) from paleosols.

Level (m)	Age (Ma)	$\delta^{13}C_c$ (‰)	$\delta^{18}O_c$ (‰)	$\delta^{13}C_o$ (‰)	$\delta^{13}C_s$ (‰)	Paleotemperature (°C)	Depth Bk (cm)	Burial depth (km)	Paleosol respired CO_2 (ppmv)	Atmospheric CO_2 (ppmv)	Atmospheric CO_2 (PIL)
248	12.80	−5.6	−15.0	−22.4	−16.3	9.6	34	0.72	2967	433 ± 128	1.5 ± 0.5
225	13.14	−4.3	−13.9	−22.4	−14.8	10.9	17	0.74	1728	519 ± 257	1.8 ± 0.9
183	13.76	−6.0	−15.0	−22.3	−16.8	8	42	0.77	3564	310 ± 77	1.1 ± 0.3
140	14.40	−5.9	−16.0	−22.1	−16.7	8	28	0.79	2541	203 ± 70	0.7 ± 0.3
122	14.66	−6.2	−16.1	−21.9	−17.0	8	32	0.80	2837	116 ± 37	0.4 ± 0.1
92	15.11	−5.8	−14.4	−21.9	−16.4	10.3	36	0.83	3138	291 ± 82	1.0 ± 0.3
58	15.61	−5.9	−15.5	−21.9	−16.3	11.6	115	0.86	8981	852 ± 86	3.1 ± 0.3
33	15.98	−5.4	−15.4	−21.7	−16.1	9.5	72	0.88	5813	579 ± 90	2.1 ± 0.3
23	16.13	−5.5	−15.3	−21.7	−16.0	11.2	54	0.90	4487	487 ± 97	1.7 ± 0.4

Notes: Age model is modified from Barnosky et al. (2007). Isotopic values $\delta^{13}C_c$ and $\delta^{18}O_c$ were measured from paleosol carbonate by Kent-Corson et al. (2006), but $\delta^{13}C_o$ was calculated from model of Passey et al. (2002) calibrated to Miocene hackberries (Backlund et al., 1991), and $\delta^{13}C_s$ was calculated from $\delta^{13}C_c$ using temperature fractionation of Romanek et al. (1992). Paleosol paleotemperature, depth to Bk and depth of burial are from Retallack (2007). PIL means multiple of pre-industrial level (280 ppmv after Alley et al., 2007).

growing season respired soil CO_2 level (P_s of Eq. (1)) of 8981 ppmv, using Eq. (2) derived from modern soil CO_2 observations corrected for atmospheric CO_2 (Fig. 3). The carbonate of the Bk horizon was measured as $\delta^{13}C$ −5.9‰ and $\delta^{18}O$ −15.5‰ (both vs. PDB: Kent-Corson et al., 2006), and its Bw horizon has modest alkali and alumina content (10.20 wt.% Al_2O_3, 2.14 wt.% K_2O, 0.62 wt.% Na_2O: Retallack, 2007), as in modern soils formed in mean annual temperature of 11.6 °C, using Eq. (7) (after Sheldon et al., 2002). This temperature can be used to calculate carbon isotopic composition of −16.3‰ for soil gases from which the carbonate was precipitated ($\delta^{13}C_s$ of Eq. (1)), following Eq. (6) (after Romanek et al., 1992). Two remaining variables needed for Eq. (1) are the isotopic composition of organic matter in the paleosols ($\delta^{13}C_o$), taken as −21.9‰ from the model for C_3 water-stressed vegetation at 15.6 Ma given by Passey et al. (2002), and isotopic composition of CO_2 in the atmosphere at this time ($\delta^{13}Ca$), calculated as −2.9‰, using the above organic matter value in Eq. (5) (from Arens et al., 2000). Inserting these values into Eq. (1) gives a middle Miocene spike of 852 ppmv, in contrast with near pre-industrial levels of CO_2 for other parts of the Miocene (Fig. 8).

The standard error of this estimate of atmospheric CO_2 ($S_{\overline{P_a}}$) has several components from the various transfer functions ($S_{\overline{P_r}}$ = ±893 ppmv, $S_{\overline{\delta^{13}C_r}} = \pm 0.28‰$, $S_{\overline{T}} = \pm 4.4$ °C) and analytic error limits ($S_{\overline{\delta^{13}C_c}} = \pm 0.5‰$, $S_{\overline{\delta^{13}C_a}} = \pm 0.1‰$), which can be summed in quadrature for Gaussian error propagation (Eq. (8)).

$$S_{\overline{P_a}} = \sqrt{\left(\frac{\partial P_a}{\partial P_r}\cdot S_{\overline{P_r}}\right)^2 + \left(\frac{\partial P_a}{\partial T}\cdot S_{\overline{T}}\right)^2 + \left(\frac{\partial P_a}{\partial \delta^{13}C_r}\cdot S_{\overline{\delta^{13}C_r}}\right)^2 + \left(\frac{\partial P_a}{\partial \delta^{13}C_a}\cdot S_{\overline{\delta^{13}C_a}}\right)^2 + \left(\frac{\partial P_a}{\partial \delta^{13}C_c}\cdot S_{\overline{\delta^{13}C_c}}\right)^2} \quad (8)$$

Full equations for each partial derivative come from transpositions of Eqs. (1) and (6) (see Supplementary data). In this particular CO_2 determination of 852 ppmv the ±893 ppmv standard error of the respired CO_2 transfer function (Eq. (2); Fig. 3) gives ±86 ppmv atmospheric CO_2, because of the low ratio of P_a/P_r (852/8981 = 0.09). This degree of uncertainty is a considerable improvement over past guesstimates of ca. ±2000 ppmv respired soil CO_2 (Nordt et al., 2003; Ekart et al., 1999), which gives ±134 ppmv atmospheric CO_2 in this case. Trivial amounts of uncertainty come from carbonate carbon isotopic analysis (±0.05‰ giving ±0.009 ppmv atmospheric CO_2) and atmospheric CO_2 carbon isotopic composition modelled from organic carbon isotopic determination (±0.4‰ giving ±0.0013 ppmv atmospheric CO_2). Additional uncertainty comes from paleotemperature estimates, with ±0.28‰ for Eq. (6) giving ±0.02 ppmv atmospheric CO_2, and ±4.4 °C for Eq. (7) giving ±9 ppmv atmospheric CO_2. Thus middle Miocene atmospheric CO_2 is here estimated at 852 ± 86 ppmv, or ±0.31 PIL (pre-industrial level of 280 ppmv: Alley et al., 2007). The middle Miocene CO_2 spike was at least 666 ppmv, significantly greater than pre-industrial (280 ppmv) and 2008 (386 ± 2 ppmv standard deviation of seasonal variation) levels of atmospheric CO_2.

4.5. Comparison with other Miocene CO_2 estimates

New CO_2 estimates from Idaho paleosols presented here (Fig. 8E) support stomatal-index estimates (Fig. 8F) of high middle Miocene atmospheric CO_2 (Retallack, 2002; Kürschner et al., 2008). Error of isotopic analyses is small (<0.05‰), unlike stomatal-index measurements, which have large standard deviations (typically 1% in measures that range from 5 to 12%: Retallack, 2001; Kürschner et al., 2008). Also compatible with estimates presented here are 2–7 PIL CO_2 from thermodynamic modelling of base depletion in middle Miocene intrabasaltic paleosols from Oregon (Sheldon, 2006c).

In contrast, these new results are very different from marine alkenone (Pagani, 2002) and boron (Pearson and Palmer, 1999) paleobarometers (Fig. 8F), and their attendant implications of CO_2–climate uncoupling (Cowling, 1999). The alkenone and boron paleobarometers had sensitivity and other limitations anyway (discussed at length by Retallack, 2002; Royer et al., 2001). The middle Miocene CO_2 greenhouse spike in Idaho–Montana had higher precipitation and temperature as predicted by greenhouse theory (Fig. 8A–D), and these changes were globally widespread because they are reflected in marine stable isotopic records (Fig. 8G–H). The climate and atmosphere of the middle Miocene is thus the most recent analog for the world predicted for 2100 by current models of atmospheric CO_2 pollution (Alley et al., 2007).

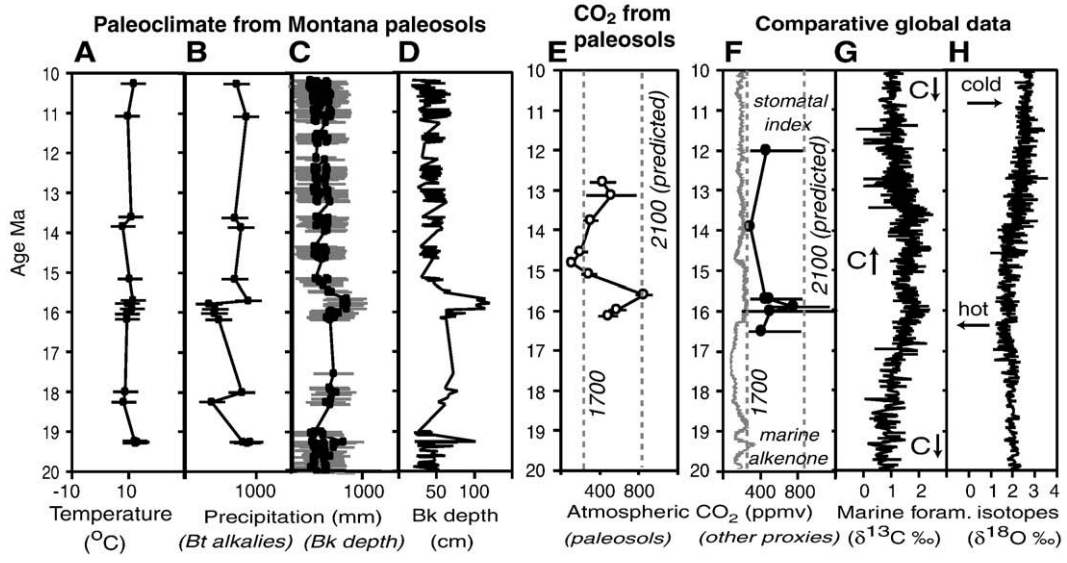

Fig. 8. Middle Miocene greenhouse and climate change in Railroad Canyon, Idaho, compared with some global change proxies: A, mean annual paleotemperature (°C) of Idaho–Montana paleosols using alkali ratios; B–C, mean annual precipitation (mm) of Idaho–Montana paleosols from CIA-K index of Bt horizon (B) and from compaction corrected depth to Bk horizon (C); D, uncorrected depth to Bk in paleosols (cm); E–F, atmospheric CO_2 (ppmv) calculated from pedogenic carbonate carbon isotopic values corrected for soil respiration from depth to Bk (E) and from marine alkenone isotopic values (F, North Atlantic site 608, after Pagani, 2002) and stomatal index of fossil *Ginkgo* (F, from Retallack 2002; Kürschner et al., 2008); G–H, carbon and oxygen isotopic composition of benthic foraminifera (after Zachos et al., 2001). Errors in E–F are a standard errors from the transfer function used (A–C, E), except for stomatal index which is two standard deviations of measurement variation (F).

5. Conclusions

Past estimation of atmospheric CO_2 from pedogenic carbonate isotopic composition of paleosols was compromised by unknown respired CO_2 concentrations of paleosols (Cerling, 1991). Relationships between depth to calcic or gypsic horizon in modern soils and respired soil CO_2 concentration (Fig. 3) can now be used to estimate respired soil CO_2 concentration in paleosols, after correction for compaction during burial (Sheldon and Retallack, 2001b). This and refinements of the pedogenic carbonate CO_2 paleobarometer for temperature and atmospheric isotopic variation are here demonstrated with a worked example of fluctuations in atmospheric CO_2 during the middle Miocene (Fig. 8). This and other refinements of the Cerling (1991) CO_2 paleobarometer give estimates of atmospheric CO_2 from paleosols (maximum at 15.6 Ma of 852 ± 86 ppmv) comparable with estimates from stomatal index of fossil plants (Kürschner et al., 2008), but with less standard error. Calcareous paleosols have additional advantages of much greater temporal resolution (Retallack, 2007) than plants with preserved cuticle (Retallack, 2002). Calcareous paleosols are now known as old as 2.6 Ga (Watanabe et al., 2000), and supplement mass balance approaches to non-calcareous paleosols for calculating atmospheric CO_2 during the Precambrian (Sheldon, 2006a). Paleosol records can thus be extended further back in time than CO_2 proxies based on foraminifera (Pearson and Palmer, 1999; Pagani, 2002). Calcareous paleosols reveal short-lived spikes in atmospheric CO_2 (Fig. 8), not apparent in geochemical approaches of coarse temporal resolution (Rothman, 2002; Berner, 2006), and are more accurate proxies of CO_2 than marine algal carbon isotopic composition (Kaufman and Xiao, 2003).

Acknowledgements

Douglas Ekart, Neil Tabor, Lee Nordt, and Nathan Sheldon offered helpful discussions, Dan Breecker furnished data and advice, and three anonymous reviewers gave invaluable advice. Work was funded by University of Oregon Summer Faculty Award.

Appendix A. Supplementary data

Supplementary data associated with this article can be found in the on line version at doi: 10.1016/j.palaeo.2009.07.011.

References

Alley, R., Berntsen, T., Bindoff, N.I., et al., 2007. Climate Change 2007: The Physical Science Basis. Intergovernmental Panel on Climate Change, Geneva.
Arens, N.C., Jahren, A.H., Amundson, R., 2000. Can C3 plants faithfully record the carbon isotopic composition of atmospheric carbon dioxide? Paleobiology 26, 137–164.
Backlund, D., Gabel, M.L., Tieszen, L.L., 1991. An environmental gradient in the Tertiary Great Plains as indicated by stable carbon isotopes from organic carbon in plant fossils. South Dakota Acad. Sci. 70, 99–108.
Barnosky, A.D., Labar, W.J., 1989. Mid-Miocene (Barstovian) environmental and tectonic setting near Yellowstone Park. Wyoming and Montana. Geol. Soc. Amer. Bull. 101, 1448–1456.
Barnosky, A.D., Bibi, F., Hopkins, S.B., Nichols, R., 2007. Biostratigraphy and magnetostratigraphy of the mid-Miocene Railroad Canyon sequence, Montana and Idaho, and age of the mid-Tertiary unconformity west of the continental divide. J. Vertebrate Paleont. 27, 204–224.
Behrensmeyer, A.K., Quade, J., Cerling, T.E., Kappelman, J., Khan, I.A., Copeland, P., Roe, L., Hicks, J., Stubblefield, P., Welles, S.J., Latorre, C., 2007. The structure and rate of late Miocene expansion of C4 plants: evidence from lateral variation in stable isotopes in paleosols of the Siwalik Group, northern Pakistan. Geol. Soc. Amer. Bull. 119, 1486–1505.
Berner, R.A., 1997. The rise of land plants and their effects on weathering and atmospheric CO_2. Science 276, 543–546.
Berner, R.A., 2006. GEOCARBSULF; a combined model for Phanerozoic atmospheric O_2 and CO_2. Geochim. Cosmochim. Acta 70, 5653–5664.
Borup, H.J., 2004. Soil Survey of Nye County, Nevada, Southwest Part. US Dept. Agriculture, Washington DC.
Breecker, D.O., Sharp, Z.D., McFadden, L.D., 2009. Seasonal bias in the formation and stable isotopic composition of pedogenic carbonate in modern soils from central New Mexico, USA. Geol. Soc. Amer. Bull. 121, 630–640.
Brook, G.A., Folkoff, M.E., Box, E.O., 1983. A world model of soil carbon dioxide. Earth Surface Processes Landforms 8, 79–88.
Bruch, A.A., Uhl, D., Mosbrugger, V., 2007. Miocene climate in Europe; patterns and evolution; a first synthesis of NECLIME. Palaeogeogr. Palaeoclim. Palaeoec. 253, 1–7.
Burbank, D.W., Barnosky, A.D., 1990. The magnetostratigraphy of Barstovian mammals in southwestern Montana and implications for the initiation of Neogene crustal extension in the northern Rocky Mountains. Geol. Soc. Amer. Bull. 102, 1093–1104.
Buyanovsky, G.A., 1972. Osobennosti rezhima CO_2 gazovoi faze cil'nokarbonatnikh pochv (CO_2 regime in gaseous phases of calcareous soils). Pochvovedenie 9, 82–88.
Buyanovsky, G., Dicke, M., Berwick, P., 1982. Soil environment and activity of soil microflora in the Negev desert. J. Arid Environ. 5, 13–28.
Cande, S.C., Kent, D.V., 1995. Revised calibration of the geomagnetic polarity timescale for the Late Cretaceous and Cenozoic. J. Geophys. Res. B100, 6093–6095.
Cerling, T.E., 1991. Carbon dioxide in the atmosphere: evidence from Cenozoic and Mesozoic paleosols. Amer. J. Sci. 291, 377–400.
Clayton, J.S., Ehrlich, W.A., Cann, D.B., et al., 1977. Soils of Canada, vol. 1. Canada Dept. Agric. Soil Rept, Ottawa.
Cochran, C.C., Richardson, M.L., 2003. Soil Survey of Pima County, Arizona, Eastern Part. Government Printer, Washington DC.
Cowling, S.A., 1999. Plants and temperature; CO_2 uncoupling. Science 285, 1500–1501.
Dan, J., Moshe, R., Alperovich, N., 1973. The soils of Sede Zin. Israel J. Earth Sci. 22, 211–227.
de Jong, E., 1981. Soil aeration as affected by slope position and vegetative cover. Soil Sci. 131, 34–43.
de Jong, E., Schappert, H.J.V., 1972. Calculation of soil respiration and activity from CO_2 profiles in the soil. Soil Sci. 113, 328–333.
Demkin, V.A., Yakimov, A.S., Alekseev, A.O., et al., 2006. Paleosol and paleoenvironmental conditions in the Lower Volga Steppes during the Golden Horde Period (13th–14th centuries AD). Eurasian Soil Sci. 39, 115–126.
Dworkin, S.I., Nordt, L., Atchley, S., 2005. Determining terrestrial paleotemperature using the oxygen isotopic composition of pedogenic carbonate. Earth Planet. Sci. Lett. 237, 56–68.
Ekart, D.P., Cerling, T.E., Montañez, I.P., et al., 1999. A 400-million-year carbon isotope record of pedogenic carbonate: implications for paleoatmospheric carbon dioxide. Amer. J. Sci. 299, 805–827.
Ghosh, P., Eiler, J., Campana, S.E., Feeney, R.F., 2007. Calibration of the carbonate 'clumped isotope' paleothermometer for otoliths. Geochim. Cosmochim. Acta 71, 2736–2744.
Hanneman, D.L., Wideman, C.J., 2006. Calcic pedocomplexes—regional sequence boundary indication in Tertiary deposits of the Great Plains and western United Staes. In: Alonso-Zarza, A.M., Tanner, L.H. (Eds.), Paleoenvironmental Record and Applications of Calcretes and Palustrine Carbonates. Geol. Soc. Amer.Spec. Pap., 416, pp. 1–15.
Kaufman, A.J., Xiao, S., 2003. High CO_2 levels in the Proterozoic atmosphere estimated from analyses of individual microfossils. Nature 425, 279–282.
Kent-Corson, M.L., Sherman, L.S., Mulch, A., Chamberlain, C.P., 2006. Cenozoic topographic and climatic response to changing tectonic boundary conditions in western North America. Earth Planet. Sci. Lett. 252, 453–466.
Kürschner, W.M., Kvaček, Z., Dilcher, D.L., 2008. The impact of Miocene atmospheric carbon dioxide fluctuations on climate and the evolution of terrestrial ecosystems. Nat. Acad. Sci. U.S. Proc. 105, 449–453.
Lieth, H., Whitakker, R.H., 1975. Primary productivity of the biosphere. Springer, New York.
Matsevich, V.B., 1957. Rezhim uglekisloti v pochvennom vozdukhe steli i polupulstini pod drevesnimi i travyanistimi tsenozami (Carbon dioxide regime in soil air of steppe and semi-desert under tree and herbaceous coenoses). Voprosy Agronomicheskoi Fiziki 95, 264–275.
Matsumoto, E., Naruoka, T., da Silva, E.F., 1997. Concentration of carbon dioxide in regolith air in different tropical geoecosystems of northeast Brazil. Inst. Geosci. Univ. Tsukuba Ann. Rept. 23, 11–15.
McElwain, J.C., Beerling, D.J., Woodward, F.J., 1999. Fossil plants and global warming at the Triassic–Jurassic boundary. Science 285, 1386–1390.
McFadden, L.D., Tinsley, J.C., 1985. Rate and depth of pedogenic-carbonate accumulation in soils: formulation and testing of a compartment model. In: Weide, D.L. (Ed.), Soils and Quaternary geology of the southwest United States. Geol. Soc. Amer. Spec. Pap. 203, 23–41.
Mikhailova, E.A., Bryant, R.B., Vassenev, I.I., et al., 2000. Cultivation effects on soil carbon and nitrogen contents at depth in the Russian Chernozem. Soil Sci. Soc. Amer. Proc. 64, 738–745.
Montañez, I.P., Tabor, N.J., Niemeier, D., et al., 2007. CO_2 -forced climate and vegetation instability during late Paleozoic deglaciation. Science 315, 87–91.
Mora, C.I., Driese, S.G., Seagar, P.G., 1991. Carbon dioxide in the Paleozoic atmosphere: evidence from carbon isotopes of pedogenic carbonate. Geology 19, 1017–1020.
Mora, C.I., Sheldon, B.T., Elliott, W.C., Driese, S.G., 1998. An oxygen isotope study of illite and calcite in three Appalachian Paleozoic vertic paleosols. J. Sedim. Res. 68, 456–464.
Nordt, L., Atchley, S., Dworkin, S., 2003. Terrestrial evidence for two greenhouse events in the latest Cretaceous. GSA Today 13 (12), 4–9.
Ogg, J.G., Smith, A.G., 2004. The geomagnetic polarity time scale. In: Gradstein, F.M., Ogg, J.G., Smith, A.G. (Eds.), A Geologic Time Scale 2004. Cambridge, Cambridge University Press, pp. 63–96.
Pagani, M., 2002. The alkenone-CO_2 proxy and ancient atmospheric carbon dioxide. Roy. Soc. London Phil. Trans. 360, 609–632.
Pagani, M., Arthur, M.A., Freeman, K.H., 1999. Miocene evolution of atmospheric carbon dioxide. Paleoceanography 14, 273–292.

Parada, C.B., Long, A., Davis, S.N., 1983. Stable isotope composition of soil carbon dioxide in the Tucson Basin, Arizona, USA. Isotope Geoscience 1, 219–236.
Passey, B.H., Cerling, T.H., Perkins, M.E., et al., 2002. Environmental change in the Great Plains: an isotopic record from fossil horses. J. Geol. 110, 123–140.
Pearson, P.N., Palmer, M.R., 1999. Middle Eocene seawater pH and atmospheric carbon dioxide concentrations. Science 284, 1824–1826.
Pearson, P.N., Palmer, M.R., 2000. Atmospheric carbon dioxide concentrations over the past 60 million years. Nature 406, 695–699.
Prothero, D.R., Draus, E., Foss, S.E., 2006. Magnetic stratigraphy of the lower portion of the middle Miocene Mascall Formation, central Oregon. Paleobios 26, 37–42.
Quade, J., Cerling, T.E., Bowman, J.R., 1989. Systematic variations in the carbon and oxygen isotopic composition of pedogenic carbonate along elevation transects in the southern Great Basin, United States. Geol. Soc. Amer. Bull. 101, 464–475.
Retallack, G.J., 1997. A Colour Guide to Paleosols. Wiley, Chichester.
Retallack, G.J., 2001. Soils of the Past. Blackwell, Oxford.
Retallack, G.J., 2002. Carbon dioxide and climate over the past 300 Myr. Roy. Soc. London Phil. Trans. 360, 659–673.
Retallack, G.J., 2005. Pedogenic carbonate proxies for amount and seasonality of precipitation in paleosols. Geology 33, 333–336.
Retallack, G.J., 2007. Cenozoic paleoclimate on land in North America. J. Geol. 115, 271–294.
Retallack, G.J., 2008. Cambrian paleosols and landscapes of South Australia. Austral. J. Earth Sci. 55, 1083–1106.
Romanek, C., Grossman, E., Morse, J., 1992. Carbon isotopic fractionation in synthetic aragonite and calcite: effects of temperature and precipitation rate. Geochim. Cosmochim. Acta 56, 419–430.
Rothman, D.H., 2002. Atmospheric carbon dioxide levels for the last 500 million years. Nat. Acad. Sci. U.S.A. Proc. 99, 4167–4171.
Royer, D.L., Berner, R.A., Beerling, D.J., 2001. Phanerozoic atmospheric CO2 change: evaluating geochemical and paleobiological approaches. Earth Sci. Rev. 54, 349–392.
Sage, R.F., Weedin, O.A., Li, M., 1999. Biogeography of C_4 photosynthesis: pattern and controlling factors. In: Sage, R.F., Monson, R.K. (Eds.), Plant biology. San Diego, Academic, pp. 313–373.
Salayev, M.E., 1985. Khimicheski i mineralogicheskiy sostav tselinnykh oroshayemykh pochv (Chemical and mineralogical composition of virginal and irrigated soils of Mil Plain). Akademiya Nauk Azerbaidzhanskoi SSR 41 (2), 74–77.
Sheldon, N.D., 2006a. Precambrian paleosols and atmospheric CO_2 levels. Precambrian Res. 147, 148–155.
Sheldon, N.D., 2006b. Quaternary glacial–interglacial climate cycles in Hawaii. J. Geol. 114, 367–376.
Sheldon, N.D., 2006c. Using paleosols of the Picture Gorge Basalt to reconstruct the middle Miocene climatic optimum. PaleoBios 26, 27–36.
Sheldon, N.D., Retallack, G.J., 2001. Equation for compaction of paleosols due to burial. Geology 29, 247–250.
Sheldon, N.D., Tabor, N.T., 2009. Quantitative paleoenvironmental and paleoclimatic reconstruction using paleosols. Earth Science Reviews 95, 1–52.
Sheldon, N.D., Retallack, G.J., Tanaka, S., 2002. Geochemical climofunctions from North American soils and application to paleosols across the Eocene–Oligocene boundary in Oregon. J. Geology 110, 687–696.
Soil Survey Staff, 2000. Keys to Soil Taxonomy. Pocahontas Press, Blacksburg, Virginia.
Tabor, N.J., 2007. Permo-Pennsylvanian palaeotemperatures from Fe-oxide and phyllosilicate $\delta^{18}O$ values. Earth Planet. Sci. Lett. 253, 159–171.
Tabor, N.J., Montañez, I.P., 2005. Oxygen and hydrogen isotope composition of Permian pedogenic phyllosilicates: development of modern surface domain arrays and implications for paleotemperature reconstruction. Palaeogeogr. Paleoclim. Paleoec. 223, 127–146.
Tabor, N.J., Yapp, C.J., 2005. Coexisting goethite and gibbsite from a high-paleolatitude (55° N) late Paleocene laterite; concentration and $^{13}C/^{12}C$ ratios of occluded CO_2 and associated organic matter. Geochim. Cosmochim. Acta 69, 5495–5510.
Tedford, R.H., Albright, L.B., Barnosky, A.D., et al., 2004. Mammalian biochronology of the Arikareean through Hemphillian interval (late Oligocene through early Pliocene epochs). In: Woodburne, MO. (Ed.), Late Cretaceous and Cenozoic Mammals of North America. Columbia University Press, New York, pp. 169–231.
Torn, M.S., Lapenis, A.G., Timofeev, A., et al., 2002. Organic carbon and carbon isotopes in modern and 100-year-old soil archives of the Russian steppe. Global Change Biology 8, 941–953.
Watanabe, Y., Martini, J.E.J., Ohmoto, H., 2000. Geochemical evidence for terrestrial ecosystems 2.6 billion years ago. Nature 408, 574–578.
Wynn, J.G., 2007. Carbon isotope fractionation during decomposition of organic matter in soils and paleosols; implications for paleoecological interpretations of paleosols. Palaeogeogr. Palaeoclim. Palaeoec. 251, 437–448.
Yapp, C.J., Poths, H., 1992. Ancient atmospheric CO_2 pressures inferred from natural goethites. Nature 355, 342–344.
Zachos, J., Pagani, M., Sloan, L., et al., 2001. Trends, rhythms, and aberrations in global climate 65 Ma to present. Science 292, 686–693.